Article

Scan-Rate-Dependent Melting Transitions of Interleukin-1 Receptor (Type II): Elucidation of Meaningful Thermodynamic and Kinetic Parameters of Aggregation Acquired from DSC Simulations

Richard L. Remmele,, Jian Zhang-van Enk, Vasu Dharmavaram, David Balaban, Mark Durst, Alex Shoshitaishvili, and Hugh Rand

J. Am. Chem. Soc., **2005**, 127 (23), 8328-8339• DOI: 10.1021/ja043466g • Publication Date (Web): 20 May 2005

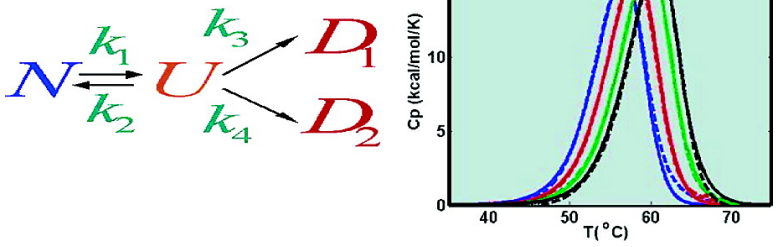

More About This Article

Additional resources and features associated with this article are available within the HTML version:

- Supporting Information
- Links to the 7 articles that cite this article, as of the time of this article download
- Access to high resolution figures
- Links to articles and content related to this article
- Copyright permission to reproduce figures and/or text from this article

View the Full Text HTML

J|A|C|S
ARTICLES
Published on Web 05/20/2005

Scan-Rate-Dependent Melting Transitions of Interleukin-1 Receptor (Type II): Elucidation of Meaningful Thermodynamic and Kinetic Parameters of Aggregation Acquired from DSC Simulations

Richard L. Remmele, Jr.,* Jian Zhang-van Enk, Vasu Dharmavaram, David Balaban, Mark Durst, Alex Shoshitaishvili, and Hugh Rand†

Contribution from Amgen Inc., One Amgen Center Drive, Thousand Oaks, California 91320-1799

Received October 28, 2004; E-mail: remmeler@amgen.com

Abstract: The role of thermal unfolding as it pertains to thermodynamic properties of proteins and their stability has been the subject of study for more than 50 years. Moreover, exactly how the unfolding properties of a given protein system may influence the kinetics of aggregation has not been fully characterized. In the study of recombinant human Interleukin-1 receptor type II (rhuIL-1R(II)) aggregation, data obtained from size exclusion chromatography and differential scanning calorimetry (DSC) were used to model the thermodynamic and kinetic properties of irreversible denaturation. A break from linearity in the initial aggregation rates as a function of $1/T$ was observed in the vicinity of the melting transition temperature ($T_m \approx 53.5$ °C), suggesting significant involvement of protein unfolding in the reaction pathway. A scan-rate dependence in the DSC experiment testifies to the nonequilibrium influences of the aggregation process. A mechanistic model was developed to extract meaningful thermodynamic and kinetic parameters from an irreversibly denatured process. The model was used to simulate how unfolding properties could be used to predict aggregation rates at different temperatures above and below the T_m and to account for concentration dependence of reaction rates. The model was shown to uniquely identify the thermodynamic parameters ΔC_P (1.3 ± 0.7 kcal/mol-K), ΔH_m (74.3 ± 6.8 kcal/mol), and T_m with reasonable variances.

1. Introduction

Aggregation of proteins can occur as a consequence of conformational alterations attributed to denaturation.[1] In this context, the term "denaturation" refers to "a process (or sequence of processes) in which the conformation of polypeptide chains within the molecule are changed from that typical of the native protein to a more disordered arrangement".[2] Denaturation can result when conformationally perturbed by temperature, pH, or chemical denaturants.[1,3,4] Aside from compromising the integrity of the protein, aggregation can often lead to decreased solubility and elicit immunogenic responses in therapeutic settings.[5−7] The importance in understanding this phenomena therefore has broad implications not only in the realm of biochemistry, but also in the world of protein therapeutics.

The process of protein aggregation can be characterized by thermodynamic and kinetic parameters.[8,9] The thermodynamic component characterizes the tendency for a given protein to unfold, resulting in a change of state. In many cases, the unfolded state can lead to an irreversibly denatured aggregate state that is kinetically controlled.[10,11] The kinetic component expresses how unfolding contributes to the overall mechanism leading to aggregation (or irreversibly denatured state). In theory, aggregation is expected to be a second-order process and therefore highly dependent on protein concentration. Moreover, because aggregation can involve multiple interactions between two or more molecules of protein, the aggregation reaction could in some cases be even greater than second-order.[8] Aggregation can also be rate-limited by the formation of an aggregation-competent state that follows first-order reaction kinetics.[12]

The premise for unfolding mediated aggregation can be explained with the knowledge that protein unfolding typically exposes buried hydrophobic regions of the molecule that become

† At 1201 Amgen Court West, Seattle, WA 98119-3105.

(1) Joly, M. *A Physico-Chemical Approach to the Denaturation of Proteins*; Academic Press: London, 1965.
(2) Kauzmann, W. *Adv. Protein Chem.* **1959**, *14*, 1−64.
(3) Remmele, R. L., Jr.; Bhat, S. D.; Phan, D. H.; Gombotz, W. R. *Biochemistry* **1999**, *38*, 5241−5247.
(4) Speed-Ricci, M.; Sarkar, C. A.; Fallon, E. M.; Lauffenburger, D. A.; Brems, D. N. *Protein Sci.* **2003**, *12*, 1030−1038.
(5) Pinckard, R. N.; Weir, D. M.; McBride, W. H. *Clin. Exp. Immunol.* **1967**, *2*, 331−341.
(6) Moore, W. V.; Leppert, P. *J. Clin. Endocrinol. Metab.* **1980**, *51*, 691−697.
(7) Robbins, D. C.; Cooper, S. M.; Fineberg, S. E.; Mead, P. M. *Diabetes* **1987**, *36*, 838−841.
(8) Krishnamurthy, R.; Manning, M. C. *Curr. Pharm. Biotechnol.* **2002**, *3*, 361−371.
(9) Grinberg, V. Y.; Burova, T. V.; Haertle, T.; Tolstoguzov, V. B. *J. Biotechnol.* **2000**, *79*, 269−280.
(10) Vermeer, A. W. P.; Norde, W. *Biophys. J.* **2000**, *78*, 394−404.
(11) Sánchez-Ruiz, J. M.; López-Lacomba, J. L.; Cortijo, M.; Mateo, P. L. *Biochemistry* **1988**, *27*, 1648−1652.
(12) Kendrick, B. S.; Carpenter, J. F.; Cleland, J. L.; Randolph, T. W. *Proc. Natl. Acad. Sci. U.S.A.* **1998**, *95*, 14142−14146.

10.1021/ja043466g CCC: $30.25

reactive in regard to associations between neighboring molecules that have also unfolded in like manner (via hydrophobic−hydrophobic interactions).[13] In this respect, the change in state is the transition from the compact or native state to the unfolded or conformationally denatured state. The kinetics that describe the system can indicate how susceptible the unfolded state is to the interaction between adjacent molecules to form complexes. Such systems were recognized by Lumry and Eyring[14] and modeled as three-state systems that involved first an unfolding event followed by an irreversibly denaturing process. The model may be described by the following scheme:

$$N \underset{k_2}{\overset{k_1}{\rightleftharpoons}} U \xrightarrow{k_3} D$$

where N is the native state, U is the unfolded (conformationally denatured) state, and D is the irreversibly denatured state or aggregation product of the reaction. The scheme represented can be described in terms of the kinetics associated with the rates of the forward and reverse reactions (k_1 and k_2) and for the irreversibly denatured or aggregate state (k_3). The kinetics of the equilibrium between the native and unfolded states are also related to the thermodynamics of the reaction since the equilibrium constant may be described as a function of the rates, k_1 and k_2,

$$K_{12} = [U]/[N] = k_1/k_2 \quad (1)$$

Building upon this premise, it would seem likely that reactions that are dependent upon an unfolding step should exhibit non-Arrhenius profiles producing curvature in the vicinity of the denaturation temperature (or melting temperature, T_m). The temperature of denaturation can be determined accurately using microcalorimetry when the system is fully reversible and when the scan rate does not exceed the rate of unfolding.[15,16] In cases where the system is irreversible, the determination is more complicated and does not lend itself to thermodynamic treatment. Furthermore, if the kinetics of the aggregation process are dependent upon unfolding, a change in kinetic behavior that coincides with the T_m of the unfolding transition should be apparent. Finally, a microcalorimetric scan rate dependence of the T_m is expected if the scheme above is applicable and kinetically controlled.[9]

One of the central limitations of classic or extended Lumry−Eyring theory for modeling protein aggregation rates is the need to generalize reaction mechanisms. Given this limitation, is it possible to extract meaningful information about the important contributing parameters that govern protein aggregation rates? The idea that scan-rate-dependent unfolding studies using microcalorimetry could be used to extract kinetic information from reactions that depend on conformationally altered states had been proposed (but not experimentally tested) in the 1980s by Privalov and Potekhin.[17] Approaches for extracting meaningful enthalpies from irreversible microcalorimetric experiments of protein unfolding have been previously reported.[18] Sánchez-Ruiz and co-workers made the generalization that, in a kinetically controlled process where the intermediate or "*U*" state was negligibly populated (as in the case for completely irreversible protein unfolding reactions where $k_3 \gg k_1$), the three-state Lumry−Eyring model could be simplified to approximate a first-order reaction from which reliable activation energies that followed Arrhenius behavior could be obtained.[11] Later building upon this work, Lepock and co-workers applied the classic three-state Lumry−Eyring model to simulate varied rate constant perturbations imposed upon thermodynamic and kinetically controlled steps associated with the unfolding thermogram properties of microcalorimetry data.[16] Finally, Roberts applied a more general theoretical approach taking into account first-, second-, and higher-order reaction kinetics ascribed to complex thermodynamic and kinetic properties of irreversible aggregation reactions to predict shelf life.[19,20] The present work derives a theoretical treatment obtained from simulations of scan-rate-dependent microcalorimetry data to extract meaningful thermodynamic and kinetic parameters from a system that is predominantly irreversible and exhibits non-Arrhenius aggregation kinetics. This investigation elucidates the role of thermal unfolding as it pertains to an irreversibly aggregated process involving recombinant human Interleukin-1 receptor, type II (rhuIL-1R(II)). The study of rhuIL-1R considers the case where aggregate formation results from the association of unfolded protein forms and describes protein unfolding as prerequisite through which dimers form, becoming the precursor to all higher-order oligomerized states.

2. Material and Methods

Purified rhuIL-1R(II) was obtained as a bulk drug concentrate (∼10 mg/mL) in a phosphate-buffered saline solution (PBS: 20 mM sodium phosphate (pH 7.4), 150 mM NaCl) obtained from Immunex Corporation (now Amgen, Inc.). The protein, expressed in CHO cells, was approximately 20% glycosylated. Protein concentrations were determined spectrophotometrically at 280 nm using an experimentally determined molar extinction coefficient of 1.61 mL/mg−cm. All excipients used were reagent grade or better. The protein polypeptide molecular weight is approximately 38 kD.

2.1. Microcalorimetry. Samples were evaluated in a vp-differential scanning calorimeter (DSC) (MicroCal, Inc.) using scan rates of 0.25, 0.5, 1.0, and 1.5 °C/min. Protein solutions were fixed at 2 mg/mL (unless otherwise noted) by diluting with the PBS-buffered solution. The T_m dependence on scan rate was assessed in the microcalorimeter using the method described by Sánchez-Ruiz and co-workers.[11]

Thermal reversibility of a 2 mg/mL solution was also examined in PBS at a scan rate of 1 °C/min within the time frame of differential heating to 90 °C, followed by cooling, re-equilibrating, and subsequently reheating a second time (time lapse between scans was essentially 1 h). The data were evaluated using Origin software (version 5.0) provided with the instrument. Transition baselines were subtracted using the "progress baseline" algorithm supplied with the software.

2.2. Time−Temperature Aggregation Studies. The temperatures selected for the time−temperature aggregation studies covered a broad range that straddled the unfolding transition endotherm. The main idea was to traverse the transition region that included temperatures well outside the transition envelope above and below the apparent melting temperature (∼58 °C at a scan rate of about 1 °C/min).

(13) Brandts, J. F. *Thermobiology*; Academic Press: New York, 1967; Chapter 3, pp 25−75.
(14) Lumry, R.; Eyring, H. *J. Phys. Chem.* **1954**, *58*, 110−120.
(15) Privalov, P. L.; Khechinashvili, N. N. *J. Mol. Biol.* **1974**, *86*, 665−684.
(16) Lepock, J. R.; Ritchie, K. P.; Kolios, M. C.; Rodahl, M.; Heinz, K. A.; Kruuv, J. *Biochemistry* **1992**, *31*, 12706−12712.
(17) Privalov, P. L.; Potekhin, S. A. *Methods Enzymol.* **1986**, *131*, 4−51.
(18) Tello-Solis, S. R.; Hernandex-Arana, A. *Biochem. J.* **1995**, *311*, 969−974.
(19) Roberts, C. J. *J. Phys. Chem. B* **2003**, *107*, 1194−1207.
(20) Roberts, C. J.; Darrington, R. T.; Whitley, M. B. *J. Pharm. Sci.* **2003**, *91*, 1095−1111.

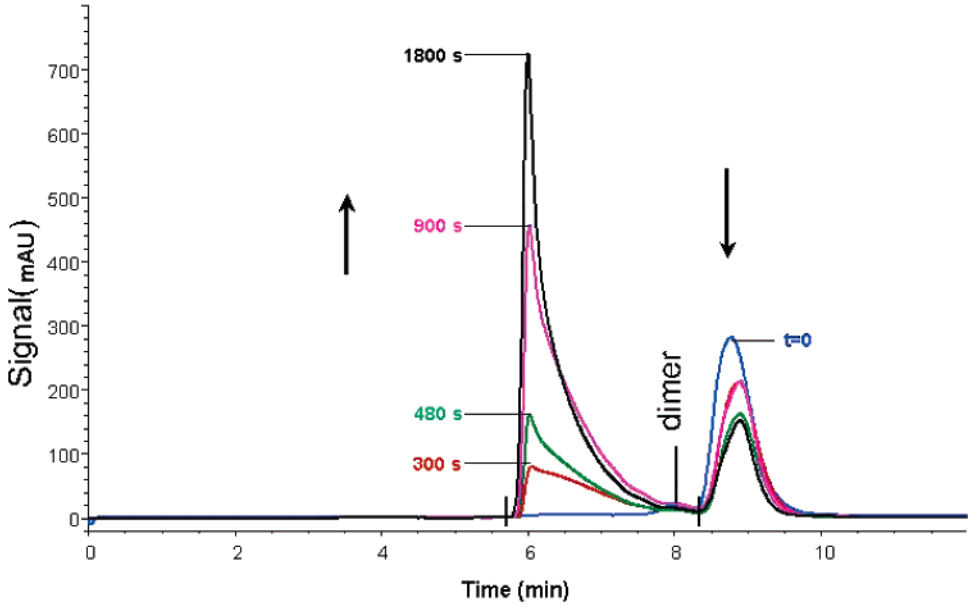

Figure 1. Illustration of unnormalized SEC results for rhuIL-1R(II) at 58 °C showing the progression of aggregates over time in seconds. Additionally, the arrows indicate the changes in the monomer (downward) and the aggregate (upward). The vertical lines bracketing elution times between 5.7 and 8.4 min represent the integration region describing total aggregation. The eluting component near 8 min is assigned to the dimer population. It is relatively stable at different temperatures and time, thus supporting the pseudo-steady-state aggregation mechanism.

The kinetics of the aggregation reaction were studied by placing 0.5 mL of protein solution in a 2-mL capacity polypropylene eppendorf vial and heating the contents at a designated temperature in an appropriate heating device (either incubator or heating block) for a designated period of time. For studies conducted using a heating block, careful attention was given to temperature control (±1 °C) and uniform heating of the sample. Bored wells (1 cm inside diameter) in an aluminum block were filled with water and allowed to equilibrate at the desired temperature prior to insertion of the eppendorf vial. At elevated temperatures ($\geq T_m$), the target temperature was reached within a 60 s interval. In the low-temperature studies (<40 °C), heating experiments were carried out in the incubator and given adequate time (2 h) to reach the equilibrium temperature prior to starting the clock. This was established by direct monitoring of the sample when temperature exhibited no greater change than ±1 °C at equilibrium with the surrounding environment. At designated time points samples were removed from the heating device, immediately placed on ice, and stored in the refrigerator before examination by size exclusion chromatography (SEC).

2.3. Size Exclusion Chromatography. Analysis was carried out on a HP-1100 HPLC system. Samples were eluted off a TosoHaas TSK-G3000 SWXL column at 1 mL/min with 100 mM phosphate (pH 6.5), 50 mM NaCl eluent. A 20-μg sample injection load was used per HPLC run. The kinetics were determined by assessing the total amount of aggregation (expressed as a percentage of the total area under the sample protein peaks) at a designated time as shown in Figure 1 for the 58 °C data as an example. The region of integration was defined by the vertical lines bracketing the elution times extending from about 5.7 to 8.4 min (Figure 1). All aggregation measurements were determined in the same way at other temperatures studied. It is noted that attention to possible competing side reactions (i.e., breakdown) was investigated and found to be negligible (no evidence) throughout the time duration of the studies presented. Hence, one could be assured that the aggregation pathway was the primary instability detected during the experiments. Furthermore, there was no evidence of protein insolubility in all cases studied herein. Detection of the eluting components was achieved with a photodiode array detector monitoring absorbance at 220 nm. The main peak eluting near 9 min and the peak eluting at 8 min were confirmed to be monomer and dimer, respectively, using the "three detector" light scattering method described previously.[21,22] It should be noted that the SEC aggregation result is assumed to accurately reflect solution state composition.

3. Theoretical Treatment

The goal of the theoretical modeling in this work was to describe the dominant underlying physical processes on a macroscopic level and to extract as accurately as possible the kinetic and thermodynamic parameters. Because many are related to each other, it is important to incorporate these relationships in the model and to use some experimentally derived quantities to cross check the consistency.

In subsequent discussions, we use the following convention for the variables and constants involved: T is temperature (in K unless otherwise noted), t is time (in minutes unless otherwise noted), G is Gibbs free energy (in kcal/mol), S is entropy (in kcal/mol/K), H is enthalpy (in kcal/mol), E is activation energy (in kcal/mol), h is enthalpy of the ensemble state (in kcal/mol), R is the gas constant (0.0019872 kcal/mol/K), k_B is the Bolzmann constant, and $\hbar$ is Planck's constant divided by 2π. Subscripts and superscripts are applied to indicate states whenever necessary.

3.1. System Description. Previous published work pertaining to the fitting or simulation of DSC experiments were described by kinetic and thermodynamic contributions.[11,16] Kinetic equations describe the rate of unfolding and aggregation reactions, while the measured thermodynamic quantity is the excess heat capacity, C_P. In the case of a two-state reversible system in steady state (see Figure 2; N is the average of the ensemble native state, and U is the average of the ensemble unfolded state[13]), the thermodynamic part can be simply described by an

(21) Wen, J.; Arakawa, T.; Talvenheimo, J.; Welcher, A. A.; Horan, T.; Kita, Y.; Tseng, J.; Nicolson, M.; Philo, J. S. *Techniques in Protein Chemistry*; Academic Press: New York, 1996; Vol. VII, pp 23−31.
(22) Wen, J.; Arakawa, T.; Philo, J. S. *Anal. Biochem.* **1996**, *35*, 155−166.

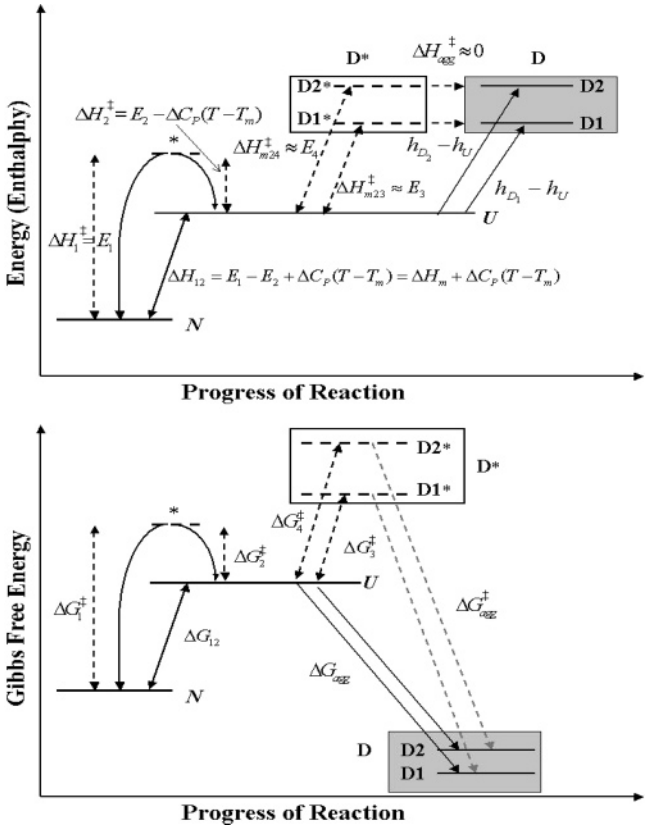

Figure 2. Proposed enthalpy and free energy diagram describing the thermal unfolding and aggregation of rhuIL-1R(II). *N*: Native state, *U*: unfolded state, D_1: aggregates formed through first-order reactions, D_2: aggregates from second-order reactions. D_1^* and D_2^* are the corresponding transition states leading to aggregation. Activation free energies related to transition states are denoted as $\Delta G_i^{\ddagger}$ (where $i = 1, 2, 3,$ or 4). The free energy of unfolding is given by ΔG_{12}, and the aggregation free energy by ΔG_{agg}. As temperature approaches T_m, ΔG_{12} goes to zero.

equilibrium constant of the unfolding reaction

$$K_{12} = \exp[-\Delta G/(RT)] = \exp[\Delta S/R - \Delta H/(RT)] \quad (2)$$

where ΔG, ΔS, and ΔH correspond to the change in Gibbs free energy, entropy, and enthalpy pertaining to the reaction, respectively. It is important to note that the thermodynamic parameter, K_{12}, can also be described in terms of the kinetic rate constants for the forward and reverse reactions as described in eq 1. The measured quantity in the DSC experiment is the excess heat capacity, $C_P(T) = [\Delta H_m + \Delta C_P(T - T_m)](-dN/dT) + \Delta C_P \cdot U(T)$[15] where the temperature increases linearly in time. The ΔC_P term is the change in heat capacity between the native and the denatured states. It has been ascribed to the exposure of hydrophobic surface to the solvent during thermal unfolding.[23] Temperature may be described in terms of the scan rate υ (°C/min) in the expression $T = T_0 + \upsilon t$ where T_0 is the initial temperature of the scan.

For a fully reversible system, thermodynamically meaningful parameters can be determined. In regard to rhuIL-1R(II), a fully reversible calorimetry experiment was nearly achieved when the protein concentration was 0.44 ± 0.04 mg/mL in a solution consisting of 2 M urea (nondenaturing by CD at 20 °C) and 0.1 M sodium phosphate for buffering at pH 7 (see inset of Figure 3). The thermodynamic quantities measured in the reversible case are $\Delta H_{cal} = 82.5 \pm 2.5$ kcal/mol, $\Delta C_p = 1.0 \pm 0.5$ kcal/mol/K, and $T_m = 325.8 \pm 0.2$ K. In this case, the $\Delta H_{cal}/\Delta H_{vh}$ ratio was ~0.9 (where ΔH_{cal} is the calorimetric and ΔH_{vh} is the van't Hoff enthalpies), suggesting the unfolding process was essentially two-state. Although urea can shift the T_m to lower temperatures and lower the enthalpy of unfolding, we have used nondenaturing levels of urea (as measured by CD at 20 °C) that should minimally perturb the unfolding transition, allowing the conditions used to represent an approximate reference point of the true T_m and associated thermodynamic parameters in the absence of the irreversible step.[24,25] The experiment showed that urea effectively blocked the progress of aggregation and that the system achieved 91% thermal reversibility in its presence. In the absence of urea, massive aggregation was observed at $T > T_m$ (Figure 4), and the process was found to be predominantly irreversible. The DSC experiment also produced different behaviors, the most prominent being an increase in the apparent melting temperature with increasing scan rates. Additionally, preliminary evidence showed that there was a negative influence in the ΔC_P on the high temperature side of the unfolding envelope. An explanation for this phenomenon affiliated with aggregation has been reported previously.[26,27]

Another important observation between the reversible and partially reversible thermal denaturation studies of rhuIL-1R(II) carried out in the DSC was the additional heat of the reaction making the total ΔH quantity higher than the urea experiment. This amounts to ~48 kcal/mol more heat in the irreversible reaction approaching a total ΔH of 130 kcal/mol (Figure 3). This would indicate that an additional endothermic contribution existed within the reaction process that involved the aggregate. It is proposed that this additional heat may arise from subsequent unfolding contributions resulting from protein−protein adsorption leading to the two *D* aggregated states of the model (as depicted in Figure 2). Such endothermic heat has been observed for bovine milk α-lactalbumin where the subprocesses of sorbent (negatively charged polystyrene latex), protein dehydration, and protein denaturation contribute to the overall driving force of surface adsorption.[28] In the case of rhuIL-1R(II), the sorbent is either another unfolded protein or soluble aggregate, and dehydration occurs by the removal of water from hydrophobic interfaces with the solvent, driving the reaction to the *D* states. In this process, a favorable increase in the entropy of the solution is expected resulting from hydrophobic surface area reduction as the aggregates continue to grow. In other words, the aggregation reaction of unfolded protein molecules in aqueous solution is an entropically driven reaction.

As for the kinetics, the SEC data shown in Figure 4 clearly indicate that there is a transition temperature where the aggregation rate of the system changes so that one cannot simply

(23) Livingston, J. R.; Spolar, R. S.; Record, T., Jr. *Biochemistry* **1991**, *30*, 4237−4244.
(24) Tanford, C.; Aune, K. C. *Biochemistry* **1970**, *9*, 206−211.
(25) Narhi, L. O.; Philo, J. S.; Sun, B.; Chang, B. S. *Pharm. Res.* **1999**, *16*, 799−807.
(26) Wiseman, T.; Williston, S.; Brandts, J. F.; Lin, L.-N. *Anal. Biochem.* **1989**, *179*, 131−137.
(27) Lin, L.-N., Mason, A. B.; Woodworth, R. C.; Brandts, J. F. *Biochemistry* **1991**, *30*, 11660−11669.
(28) Norde, W.; Haynes, C. A. In *Protein at Interfaces II. Fundamentals and Applications*; Horbet, T. A., Brash, J. L., Eds.; American Chemical Society: Washington DC, 1995; pp 26−40.

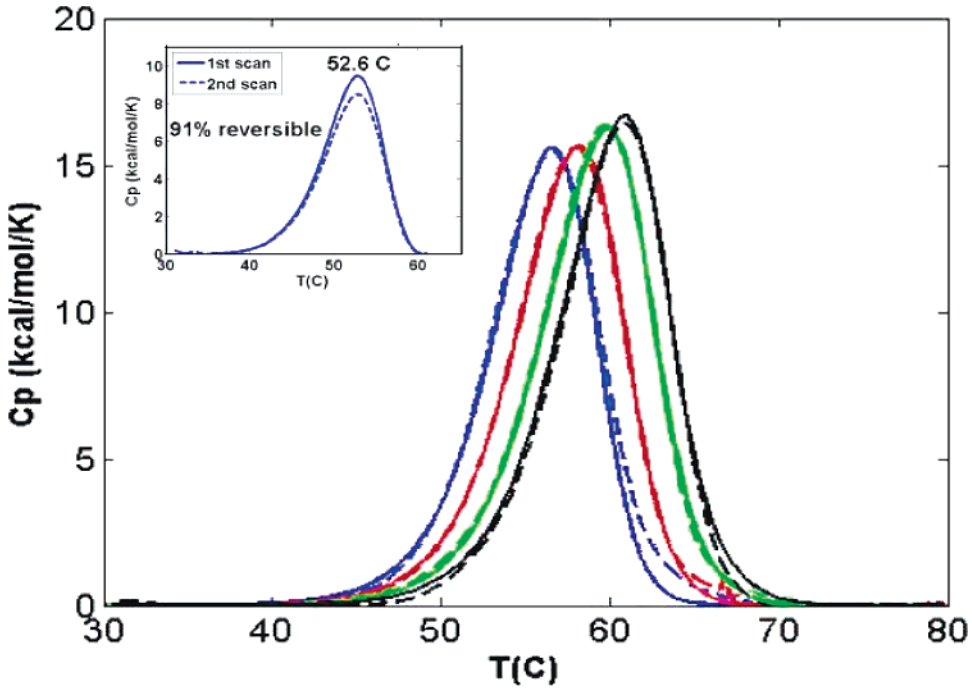

Figure 3. Comparison of the calculated result using eq 31 (solid lines) with experimental data (broken lines) for the DSC scan rate dependent experiment. From left to right, the scanning rates are 0.25, 0.5, 1.0, and 1.5 °C/min, respectively. Inset: DSC scan for a 91% reversible rhuIL-1R(II) system in 0.1 M sodium phosphate with 2 M urea, pH = 7.0. In all data shown the transition baseline has been subtracted.

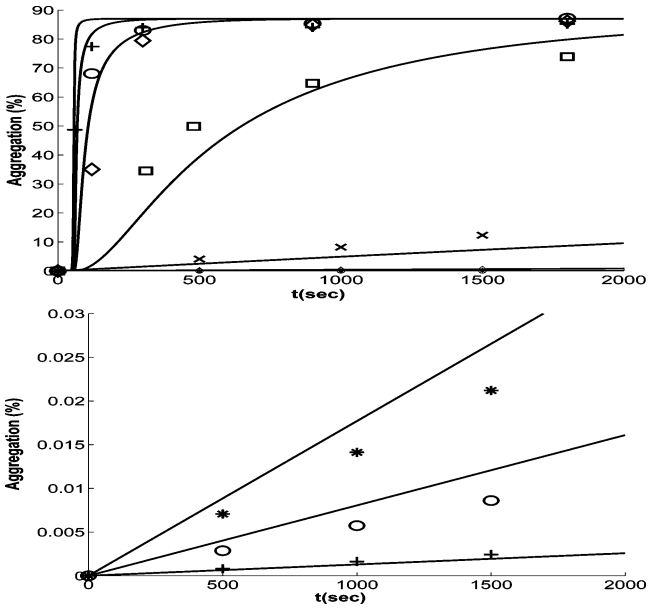

Figure 4. Time-temperature data of aggregation. The predicted fits based upon the model (eq 20) are depicted by the solid lines. Data points represented by the assorted symbols are the experimentally determined values. In the top figure, the temperatures from top to bottom are: 75, 69, 65, 58, and 50 °C. In the bottom figure, the temperatures from top to bottom are: 39, 37, and 34 °C.

explain the denaturation process in terms of a single step described by an Arrhenius rate as in the work of Sánchez-Ruiz and co-workers.[11] Nevertheless, it is still a useful model to obtain an estimated activation energy. The expanded model described by Lepock et al.[16] appears to be a better description of the system where all reactions are modeled as first-order reactions. However, our experimental observation of the concentration dependence of aggregation revealed that the approximate order of reaction was found to be 1.70 ± 0.04, suggesting that a mixture of first- and second-order reactions participate in the system. Therefore, we add to Lepock's model an extra term describing the contribution of the second-order processes. More specifically, we denote the aggregates resulting from the first-order term as D_1 and those from the second-order term as D_2. Together they are the irreversibly denatured population, D, with D_1^* and D_2^* representing the corresponding transition states that conceivably are aggregation-competent species[12] (Figure 2). The reaction can be represented by

$$N \underset{k_2}{\overset{k_1}{\rightleftharpoons}} U \begin{matrix} \overset{K_{23}}{\searrow} D_1^* \rightarrow D_1 \\ \underset{K_{24}}{\searrow} D_2^* \rightarrow D_2 \end{matrix}$$

In the pathway from $U \rightleftharpoons D_1^*$ or $U \rightleftharpoons D_2^*$, the reaction is assumed to be first-order and reversible. From $D_1^* \rightarrow D_1$ and from $D_2^* \rightarrow D_2$ the reaction follows second-order kinetics. Within the $U \rightleftharpoons D_1^* \rightarrow D_1$ path, the $U \rightarrow D_1^*$ is rate-limiting, and therefore, the overall reaction from $U \rightarrow D_1$ is first-order. Likewise, in the path from $U \rightleftharpoons D_2^* \rightarrow D_2$, the $D_2^* \rightarrow D_2$ step is rate-limiting, and therefore, the overall kinetics from $U \rightarrow D_2$ is second-order.

It should be noted in Figure 4 that at elevated temperatures above 58 °C, the reaction does not approach 100% aggregate. The data indicate a point of saturation that appears to approach 84−87%. This observation indicates that there is a remnant of protein that does not participate in the aggregation process. This remnant contribution is also observed in DSC thermal reversibility experiments and suggests that the approximate 13−16% of rhuIL-1R(II) can be accounted as fully reversible species in contrast to the majority of the molecules that go through the unfolding process leading to aggregates.

3.2. The Kinetic Equations and the Reaction Rates. Since the quantity or population of the transition state (i.e., D_1^* or

D_2^*) is short-lived, leading rapidly to the final D state (i.e., D_1 or D_2), the kinetics of the system may be represented by

$$N \underset{k_2}{\overset{k_1}{\rightleftharpoons}} U \begin{matrix} \overset{k_3}{\nearrow} D_1 \\ \underset{k_4}{\searrow} D_2 \end{matrix}$$

Assuming the total molar concentration of protein in the solution is $[N_0]$, we can normalize the molar concentration at each state by this number to get a dimensionless relative concentration:

$$N = \frac{[N]}{[N_0]} \tag{3}$$

$$U = \frac{[U]}{[N_0]} \tag{4}$$

$$D = \frac{[D]}{[N_0]} \tag{5}$$

It is important to realize that $[D]$ represents the molar concentration of irreversibly denatured protein and is defined as (aggregate weight concentration)/(monomer protein molecular weight). It is a collection of aggregate expressed as an equivalent portion of monomeric molecular forms.

The initial condition of the system is $N(t = 0) = 1$, $U(t = 0) = 0$, and $D(t = 0) = 0$. The differential equations describing the kinetics of the system are as follows:

$$\dot{N} = -k_1 N + k_2 U \tag{6}$$

$$\dot{U} = k_1 N - (k_2 + k_3)U - k_4 U^2 \tag{7}$$

$$\dot{D} = k_3 U + k_4 U^2 \tag{8}$$

where the U^2 term results from the second-order process and $D = D_1 + D_2$ with D_1 corresponding to the first-order term,[12] and D_2 corresponds to the second-order term depicting the formation of a pseudo-steady-state dimer leading to higher-order aggregates. The terms k_1, k_2, k_3, and k_4 are the corresponding rate constants.

The second-order reaction coefficient k_4 is necessarily proportional to the concentration $[N_0]$, and thus eqs 6−8 hold for any $[N_0]$. The following derivation illustrates this conclusion. Equation 7 is derived from the kinetic equation for the unnormalized concentration $[U]$:

$$[\dot{U}] = k_1[N] - (k_2 + k_3)[U] - k_4'[U]^2 \tag{9}$$

Dividing eq 9 by $[N_0]$ on both sides, one obtains

$$\frac{[\dot{U}]}{[N_0]} = k_1\frac{[N]}{[N_0]} - (k_2 + k_3)\frac{[U]}{[N_0]} - k_4'[N_0]\left(\frac{[U]}{[N_0]}\right)^2 \tag{10}$$

Now by substituting in the definitions of eqs 3−5, one arrives at

$$\dot{U} = k_1 N - (k_2 + k_3)U - (k_4'[N_0])U^2 \tag{11}$$

For eq 11 to agree with eq 7, it must be that $k_4 = k_4'[N_0]$, so that k_4' denotes a linear rate proportionality constant.

The linear dependence of k_3 on $[N_0]$ is not as obvious because it appears as a coefficient for a first-order reaction rate. Since it originates from the reaction of one unfolded molecule with any aggregate, it is reasonable to assume the same linear relation to $[N_0]$ holds true, and therefore both k_3 and k_4 can be expressed as

$$k_3 = k_3'[N_0] \tag{12}$$

$$k_4 = k_4'[N_0] \tag{13}$$

where k_3' denotes a linear rate proportionality constant analogous to k_4'. It is important to recognize that k_3 is proportional to the initial protein concentration.

The unfolding rate coefficient k_1 is known to be well-described by the Arrhenius law:[29]

$$k_1 = \exp[A_1 - E_1/(RT)] \tag{14}$$

In the experiment with urea (see the inset of Figure 3), a positive change in the baseline molar heat capacity, ΔC_P, was observed. This implies that k_2 has non-Arrhenius behavior (see eq 17), as derived from the equilibrium constant of the folding/unfolding reaction and the modified Gibbs−Helmholz equation:[30]

$$\Delta G_{12} = \Delta H_m\left(1 - \frac{T}{T_m}\right) + \Delta C_P\left[T - T_m - T\ln\left(\frac{T}{T_m}\right)\right] \tag{15}$$

From this, one can write the corresponding equilibrium constant as follows:

$$\begin{aligned} K_{12} &= \frac{k_1}{k_2} \\ &= \exp[-\Delta G_{12}/(RT)] \\ &= \exp\left\{-\left[\Delta H_m\left(1 - \frac{T}{T_m}\right) + \right.\right. \\ &\qquad \left.\left.\Delta C_P\left[T - T_m - T\ln\left(\frac{T}{T_m}\right)\right]\right]\Big/(RT)\right\} \end{aligned} \tag{16}$$

Substituting eq 14 into eq 16 and defining $E_1 - E_2 \equiv \Delta H_m$ and $A_1 - A_2 \equiv \Delta H_m/(RT_m)$ (therefore, $T_m = (E_1 - E_2)/[R(A_1 - A_2)]$) one can solve for an expression of k_2:

$$k_2 = \exp\left\{A_2 - \frac{E_2}{RT} - \frac{\Delta C_P}{R}\left[\frac{T_m}{T} - 1 + \ln\left(\frac{T}{T_m}\right)\right]\right\} \tag{17}$$

The above treatment has been well supported by experimental observations.[31] Note that it is assumed that the ΔC_P here is approximately equal to the ΔC_P measured in the experiment with urea and it is the only contribution that modifies Arrhenius rates. The term E_2 is the refolding activation energy when temperature equals T_m.

(29) Magari, R. T. *BioPharm International*, Nov 1, 2003, pp 36−48.
(30) Hu, C. Q.; Sturtevant, J. M.; Thomson, J. A.; Erickson, R. E.; Pace, C. N. *Biochemistry* **1992**, *31*, 4876−4882.
(31) Oliveberg, M.; Tan, Y. J.; Fersht, A. *Proc. Natl. Acad. Sci. U.S.A.* **1995**, *92*, 8926−8929.

The kinetic rate constants, k_3 or k_4, can be determined according to Eyring's model[32] and shown to conform to a similar expression of the form for k_2. Knowing that an equilibrium between the U and D_1^* or U and D_2^* is proposed to exist, there must be corresponding equilibrium constants K_{23} and K_{24} that describe this part of the system. These constants assume the same form as K_{12} but replace the parameters $\{\Delta H_m, T_m, \Delta C_P\}$ with $\{\Delta H_{m23}, T_{m23}, \Delta C_{P23}\}$ for k_3 and $\{\Delta H_{m24}, T_{m24}, \Delta C_{P24}\}$ for k_4. Then we multiply the resulting equilibrium constants in each case by $\kappa_x(k_BT/(2\pi\hbar))$ (where the subscript $x = 3$ or 4 corresponding to either k_3 or k_4; κ_x is the transmission coefficient). By raising the multiplication factor to an exponent, we can combine it with the exponential form of eq 16 to yield

$$k_3 = \exp\left\{\left[\frac{\Delta H_{m23}}{RT_{m23}} - \frac{\Delta C_{P23}}{R}(1 + \ln T_{m23}) + \ln\frac{\kappa_3 k_B}{2\pi\hbar}\right] - \frac{\Delta H_{m23} - \Delta C_{P23}T_{m23}}{RT} + \frac{\Delta C_{P23} + R}{R}\ln T\right\}$$

$$k_4 = \exp\left\{\left[\frac{\Delta H_{m24}}{RT_{m24}} - \frac{\Delta C_{P24}}{R}(1 + \ln T_{m24}) + \ln\frac{\kappa_4 k_B}{2\pi\hbar}\right] - \frac{\Delta H_{m24} - \Delta C_{P24}T_{m24}}{RT} + \frac{\Delta C_{P24} + R}{R}\ln T\right\}$$

The resulting k_3 and k_4 expressions are grouped to show two temperature-dependent terms and one temperature-independent constant term. The temperature-independent or constant term is enclosed within the brackets separated from the two temperature-dependent terms in the exponential. Among the temperature-dependent terms, one is inversely proportional to temperature and the other is proportional to ln T. Among the parameters ΔH_{m2x}, T_{m2x}, ΔC_{P2x}, and κ_x, we have adopted the following defined relations that transform the expressions above into equations for k_3 and k_4 that are similar to eq 17. For k_3, we define $\Delta C_P^{D_1} \equiv \Delta C_{P23} + R$, $E_3 - \Delta C_P^{D_1} T_m \equiv \Delta H_{m23} - \Delta C_{P23}T_{m23}$, and $A_3 \equiv [\Delta H_{m23}/(RT_{m23}) - \Delta C_{P23}/R(1 + \ln T_{m23}) + \Delta C_P^{D_1}/R(1 + \ln T_m) + \ln \kappa_3 k_B/(2\pi\hbar)]$. Similar relations for k_4 can be used to derive the final equations for the rate constants shown below:

$$k_3 = \exp\left(A_3 - \frac{E_3}{RT} + \frac{\Delta C_P^{D_1}}{R}\left[\frac{T_m}{T} - 1 + \ln\frac{T}{T_m}\right]\right) \quad (18)$$

$$k_4 = \exp\left(A_4 - \frac{E_4}{RT} + \frac{\Delta C_P^{D_2}}{R}\left[\frac{T_m}{T} - 1 + \ln\frac{T}{T_m}\right]\right) \quad (19)$$

Thus far, we have expressed the kinetic equations for the system in terms of a set of 11 independent parameters: $\{A_1, E_1, A_2, E_2, A_3, E_3, A_4, E_4, \Delta C_P, \Delta C_P^{D_1}, \Delta C_P^{D_2}\}$. As will be shown in the next section, the excess heat capacity can also be expressed in terms of the same set of parameters. From these parameters T_m and ΔH_m can be calculated.

3.3. The Observables: C_P and Agg. Having described the kinetic model of the system, it is important to find expressions for the excess molar heat capacity C_P and the total mass of the aggregates during the reaction in terms of these kinetic parameters.

In the time−temperature aggregation experiment, the total mass of the aggregates is proportional to $1 - N(t) - U(t)$ or D. Here aggregation is defined by the expression

$$\mathrm{Agg}(T, t) = D \quad (20)$$

It can be calculated by solving the differential eqs 6−8. From the aggregation equation (eq 20), one can derive an initial rate of aggregation as

$$R_0(T) = \left.\frac{\mathrm{d}\{\mathrm{Agg}(T, t)[N_0]\}}{\mathrm{d}t}\right|_{t=0} \approx \mathrm{Agg}(T, t_1)/t_1 \times [N_0] \quad (21)$$

where t_1 is the first time point in the measurement for a given temperature, Agg(T, 0) is assumed to be zero, and $[N_0]$ is the initial molar concentration of the protein.

In the DSC experiment, the measured quantity is the molar excess heat capacity under constant pressure. $C_P = (\partial h/\partial T)_P$ where h is the total molar excess enthalpy of the system involved in the denaturation process. In the proposed model, the states involved in the endotherm are N, U, D_1, and D_2 with $N + U + D_1 + D_2 = 1$.

$$\begin{aligned} h &= h_N N + h_U U + h_{D1} D_1 + h_{D2} D_2 - h_N \\ &= h_N N + h_U U + h_{D1} D_1 + h_{D2} D_2 - h_N(N + U + D_1 + D_2) \\ &= (h_U - h_N)U + (h_{D1} - h_N)D_1 + (h_{D2} - h_N)D_2 \end{aligned} \quad (22)$$

where h_x ($x = N$, U, D_1, D_2) are the enthalpies of the corresponding ensemble states, consisting of native, unfolded, the final aggregate states of the first- and second-order components of the reaction.

Now one can write the observed C_P more explicitly as

$$C_P(\upsilon, T) = (h_U - h_N)\frac{\partial U}{\partial T} + (h_{D1} - h_N)\frac{\partial D_1}{\partial T} + (h_{D2} - h_N)\frac{\partial D_2}{\partial T} + \frac{\partial(h_U - h_N)}{\partial T}U + \frac{\partial(h_{D1} - h_N)}{\partial T}D_1 + \frac{\partial(h_{D2} - h_N)}{\partial T}D_2 \quad (23)$$

Since the temperature is increased linearly in time for each scan rate υ, i.e., $T = T_0 + \upsilon t$, the temperature derivatives can be expressed in terms of the time derivatives and the scan rate using the chain rule, $\partial N/\partial T = \partial N/\partial t\ \partial t/\partial T = 1/\upsilon\dot{N}$. The same applies to U, D_1, and D_2. Using eqs 6−8, we can write the equation as follows:

$$C_P(\upsilon, T) = (h_U - h_N)\left(-\frac{1}{\upsilon}\dot{N}\right) + (h_{D1} - h_U)\frac{k_3}{\upsilon}U + (h_{D2} - h_U)\frac{k_4}{\upsilon}U^2 + \frac{\partial(h_U - h_N)}{\partial T}U + \frac{\partial(h_{D1} - h_N)}{\partial T}D_1 + \frac{\partial(h_{D2} - h_N)}{\partial T}D_2 \quad (24)$$

The native state is the standard state of the protein at standard temperature and pressure and an enthalpy reference point. $(h_U - h_N)$ can be expressed in terms of the unfolding

(32) Johnson, F. H.; Eyring, H.; Polissar, M. J. *The Kinetic Basis of Molecular Biology*; Wiley: New York, 1954; Introduction.

enthalpy and ΔC_P (Figure 2):

$$(h_U - h_N) = \Delta H_m + \Delta C_p(T - T_m) = E_1 - E_2 + \Delta C_p(T - T_m) \quad (25)$$

it then follows that

$$\frac{\partial(h_U - h_N)}{\partial T} = \Delta C_p \quad (26)$$

Similarly, with the assumption that no enthalpy change takes place in D^* to D transitions (see Figure 2), $(h_{D1} - h_U)$ and $(h_{D2} - h_U)$ can be determined by the equilibrium constants K_{23} and K_{24} defined in the previous section. Using the van't Hoff equation,we get

$$(h_{D1} - h_U) = -R\frac{\partial \ln K_{23}}{\partial 1/T} = \Delta H_{m23} + \Delta C_{P23}(T - T_{m23}) \approx E_3 + \Delta C_p^{D_1}(T - T_m) \quad (27)$$

$$(h_{D2} - h_U) = -R\frac{\partial \ln K_{24}}{\partial 1/T} = \Delta H_{m24} + \Delta C_{P24}(T - T_{m24}) \approx E_4 + \Delta C_p^{D_2}(T - T_m) \quad (28)$$

and consequently,

$$\frac{\partial(h_{D1} - h_N)}{\partial T} = \frac{\partial[(h_{D1} - h_U) + (h_U - h_N)]}{\partial T} = \Delta C_p^{D_1} + \Delta C_p \quad (29)$$

$$\frac{\partial(h_{D2} - h_N)}{\partial T} = \frac{\partial[(h_{D2} - h_U) + (h_U - h_N)]}{\partial T} = \Delta C_p^{D_2} + \Delta C_p \quad (30)$$

Substituting eqs 25−30 into eq 24, we have an expression for C_P in terms of scan rate and temperature:

$$C_p(\upsilon, T) = [\Delta H_m + \Delta C_p(T - T_m)]\left(-\frac{1}{\upsilon}\dot{N}\right) + \Delta C_p U + \frac{k_3}{\upsilon}[E_3 + \Delta C_p^{D_1}(T - T_m)]U + \frac{k_4}{\upsilon}[E_4 + \Delta C_p^{D_2}(T - T_m)]U^2 + (\Delta C_p^{D_1} + \Delta C_p)D_1 + (\Delta C_p^{D_2} + \Delta C_p)D_2 \quad (31)$$

The first line of eq 31 contains the familiar terms describing the two-state reversible system. The terms on the second line of eq 31 are necessary to describe the contribution of the aggregation step to the overall heat absorption. When k_3 and k_4 are zero, so are D_1 and D_2, and the equation reduces to the fully reversible case. When the sum $\Delta C_p^{D_1} + \Delta C_P$ or $\Delta C_p^{D_2} + \Delta C_P$ does not equal zero, the last two terms give a nonvanishing baseline shift that can contribute to a negative net influence on the transition baseline. The negative influence on the transition baseline can occur when $\Delta C_p^{D_1}$ or $\Delta C_p^{D_2}$ result from buried hydrophobic surface as would be expected in the aggregation process. After subtraction of the transition baseline, the last two terms in eq 31 are of no consequence. Therefore, the fitted data shown in Figure 3 are based on this equation with the last two terms excluded.

Equation 31 was used to fit the experimental data to extract all the Arrhenius parameters. Numerically speaking, a nonlinear least-squares fitting routine (*lsqnonlin* in Matlab) was applied to minimize the two sum-of-squares functions simultaneously. The first represents the difference between the calculated values and the observed values in the DSC experiment, and the second represents the difference between the calculated and observed values in the SEC experiment. Denoting the calculated values with a superscript calcd and the observed values with a superscript expt, we can write the two sum of squares functions as:

$$\chi_1 = \sum_{i=1}^{4}\sum_{j=1}^{n_i} w_i |\, C_p^{calcd}(\upsilon_i, T_j) - C_p^{expt}(\upsilon_i, T_j)|^2 \quad (32)$$

where υ_i ($i = 1, 2, 3, 4$) is the designated scan rate and n_i ($i = 1, 2, 3, 4$) represents the corresponding data points of each scan. The term w_i is an optional weighting factor to ensure each data point is counted appropriately. The reason for the weighting factor is to account for the collection of more data points at the slower scan rate than that obtained at the faster scan rate. Without weighting, each data point contributes equally to the sum-of-squares function. This leads to more contributions from the slower scan data. The weighting factor of $w_i = 1/n_i$ makes the contribution of each scan equal.

$$\chi_2 = \sum_{i=1}^{9}\sum_{j=1}^{n_i} |\, \ln[\mathrm{Agg}^{calcd}(T_i, t_j)] - \ln[\mathrm{Agg}^{expt}(T_i, t_j)]|^2 \quad (33)$$

where $i = 1-9$ represents the nine temperatures under which the aggregation experiment took place. We used $n_i = 3$, that is, the first three points at each temperature to do the fitting. Note that either χ_1 or χ_2 can be used alone for fitting the parameters. In fact, that is what was often done in the literature. But the sensitivity of the two observed quantities to each parameter is different. To best constrain the parameter space, we performed a simultaneous fitting for both. In other words, we minimized the following quantity:

$$\chi = \chi_1 + F\cdot\chi_2 \quad (34)$$

where F is an arbitrary scaling factor selected to make contributions from χ_1 and $F\cdot\chi_2$ to χ similar in order of magnitude, since the two quantities have different dimensions and would be otherwise incomparable.

We paid special attention to the question of *identifiability*, the ability to guarantee that all 11 parameters, $p = \{A_1, E_1, A_2, E_2, A_3, E_3, A_4, E_4, \Delta C_P, \Delta C_p^{D_1}, \Delta C_p^{D_2}\}$, are uniquely determined by minimizing eq 34 and consequently, T_m and ΔH_m are also identifiable with reasonable variances. (If the parameters were nonidentifiable, then different values for the 11 parameters could produce the same sum of squares.) It is not possible to guarantee this globally, but we can guarantee it locally near the calculated parameters p_0 yielding the minimum of χ (eq 34).

We used variational methods to calculate the partial derivatives

$$\frac{\partial C_p(T_i)}{\partial p_j}\Big|_{p_0}$$

for each of the 11 parameters $j = 1, ..., 11$ at each of the n temperature points T_i, $i = 1,..., n$ evaluated by the symbolic and numerical differential equation solver (in our calculations n was on the order of 200). This yielded a matrix of size 11 by n. Numerical calculation showed that the rank of this matrix

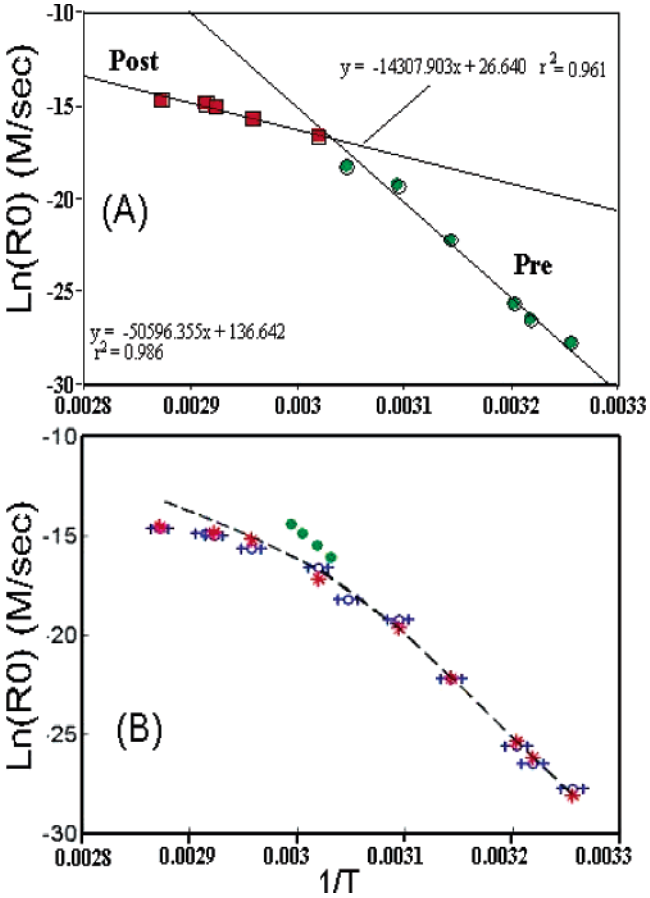

Figure 5. (A) Arrhenius plot showing the best least-squares fit of data to two distinctly different lines for pre and post unfolding transition temperature zones of rhuIL-1R(II). The crossover point of the two lines is in the vicinity of the T_m. (B) Comparison of the initial aggregation rates showing the corresponding symbols: (*) calculation based on the model (eq 21), (− − −) rate approximation ($k' = (k_1k_3)/(k_1 + k_2 + k_3)$), and (○) experimental data. The experimental error in temperature is indicated by (+) on both sides of the data points. (●) Sánchez-Ruiz et al. treatment of scan rate data.

was the maximal size of 11, ensuring the nondegeneracy of the defining equations and the identifiability of the parameters, so that the values we calculated are indeed locally uniquely determined.

4. Results and Discussions

4.1. Time−Temperature Studies. The rate of aggregation was derived from a plot showing the amount of aggregate measured by SEC as a function of time as depicted in Figure 4 using eq 21. At low temperatures between 30 and 50 °C, linear rates of reaction were easily ascertained since there was no deviation from linearity during the period of time examined. However, at temperatures >58 °C, the initial reaction rate was calculated according to eq 20. The observed rate constants obtained from these data were converted to units of M/s and then subsequently evaluated in the form of an Arrhenius plot (Figure 5A).

It has been shown that it is possible to fit the data with two lines, reflecting approximate Arrhenius behavior above and below the apparent melting temperature (as depicted in Figure 5A). The data points that determine the lines were found by optimizing both correlation coefficients. From the slope of the lines describing these two regions, one is able to characterize the aggregation reaction kinetics with two activation energies. At low temperatures (below T_m), an activation energy of 100 kcal/mol was obtained, and at high temperatures (above T_m), the activation energy was found to be approximately 28 kcal/mol.

The Arrhenius data in Figure 5A clearly show a break from linearity in the reaction rate around the melting temperature, indicating two different activation energies at two different temperature regions, separated approximately by T_m. This behavior can be explained by a rate approximation from the kinetic model (eqs 6−8). When $k_3 \ll k_2$ and $k_4 \ll k_3$ (valid at low temperatures below the T_m), the equilibrium between N and U predominates as expected, and the aggregation can be described by an effective rate coefficient $k' = (k_1k_3)/(k_1 + k_2 + k_3)$. The effective rate is plotted as the dashed line in Figure 5B. It can be seen that this approximation is very good at low temperature (when $T \ll T_m$, $k_2/k_1 \gg 1$, therefore $k' \approx k_3k_1/k_2$). When $T \gg T_m$, $k' \approx k_3$, although the rate approximation for aggregates is not as good in this temperature region, one can still obtain a qualitative estimate of k_3 from the experimental data. It should be noted that our numerical fitting was performed over the entire time sequence of study and not just limited to the initial rates. The initial rates are used to estimate the starting parameters for the nonlinear fitting and used for checking the consistency of the final results.

In the DSC experiment, the apparent melting temperature T_{app} depends on the scan rate of the irreversible system. The scan-rate-dependent activation energy of the T_{app} was also examined to ascertain the relevance to the activation energy obtained from the Arrhenius plot of the time−temperature studies. The results obtained from a plot of $\ln[v/T_{app}^2]$ as a function of $1/T_{app}$ as proposed by Sánchez-Ruiz et al.,[11] yielded a straight line with an associated activation energy of about 89 kcal/mol. This treatment appears to yield an activation energy that is consistent with the low-temperature fit in the SEC experiment, namely, a respectable result that compares well with the activation energy obtained from the time−temperature studies. For illustration purposes, the scan-rate method of Sánchez-Ruiz and co-workers[11] is plotted as solid circles in Figure 5B (within the region from 0.0029 (61.3 °C) to 0.0030 (56.9 °C)). The lower activation energy of the scan-rate-dependent result may exhibit some bias imposed by the region of curvature so that extrapolation to low temperatures would result in overestimates of aggregation reaction rates.

4.2. Theoretical Results. After performing the procedure of the nonlinear least-squares fitting outlined in the theoretical treatment section, we obtained numerical values for all the parameters in the model system. As discussed in Section 3.1, since the aggregation reaction is entropically driven, the transition from D_1^* and D_2^* to the final D_1 and D_2 states was spontaneous, driven by the removal of hydrophobically exposed surfaces during aggregation. Little or no heat was released ($\Delta H_{agg}^{\ddagger} \approx 0$) in this process, but the entropy of the solution was increased. Therefore, the change in Gibbs free energy $\Delta G_{agg}^{\ddagger}$ (see Figure 2) can be expressed as

$$\Delta G_{agg}^{\ddagger} \approx -T\Delta S_{agg}^{\ddagger} = -T(\Delta S^{\ddagger}_{D_1{}^*D_1}\cdot D_1 + \Delta S^{\ddagger}_{D_2{}^*D_2}\cdot D_2) \quad (35)$$

The relevant parameters are displayed in Table 1.

Table 1. Parameters Obtained from Fitting the Model to Both DSC Traces and SEC Aggregation Curves Simultaneously[a]

A_1 ln(1/min)	E_1 kcal/mol	A_2 ln(1/min)	E_2 kcal/mol	A_3 ln(1/min)	E_3 kcal/mol	A_4 ln(1/min)	E_4 kcal/mol
115.4 ± 1.7	76.6 ± 1.2	1.0 ± 11.7	2.3 ± 8.0	68.9 ± 6.9	46.8 ± 4.4	228.1 ± 22.6	151.7 ± 15.0

ΔH_m kcal/mol	T_m K	ΔC_P kcal/mol·K	$\Delta C_P^{D_1}$ kcal/mol·K	$\Delta C_P^{D_2}$ kcal/mol·K
74.3 ± 6.8	326.6 ± 1.4	1.3 ± 0.7	−0.2 ± 0.5	−5.8 ± 1.6

[a] Uncertainties in the parameter estimation represent those associated with an assumed 10% experimental uncertainty in protein concentration.

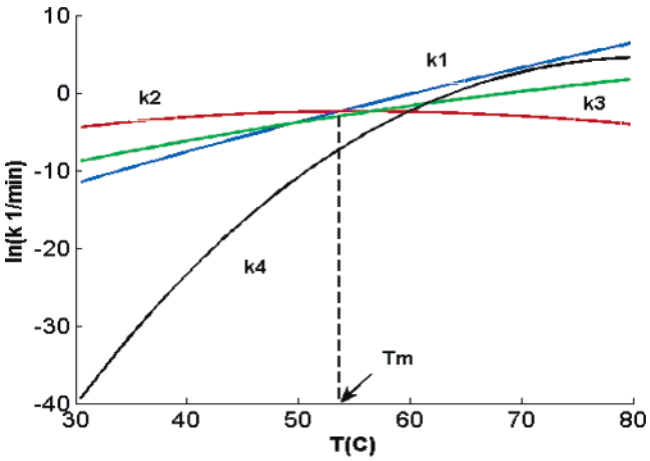

Figure 6. Temperature dependence of the kinetic rate constants for 2 mg/mL rhuIL-1R(II). The point denoting the temperature where $k_1 = k_2$ is the extracted T_m.

The rate constant profiles as a function of temperature are shown in Figure 6 with corresponding activation energies in Table 1. Considering conditions below the T_m in Figure 6, the model depicts k_4 (with associated activation energy, E_4) as least important based on a slower reaction rate and correspondingly high-energy barrier (152 kcal/mol). E_3 on the other hand with associated rate constant k_3 has a activation energy (47 kcal/mol) lower than either E_1 or E_4 and therefore predominates the aggregation pathway, rate limited only by the supply of aggregation competent species D_1^* and unfolded forms of the protein. This is explicit from the fact that k_1 is rate-limiting and slower than k_3. Hence, at temperatures below the T_m, solution conditions that tend to stabilize the native state will greatly impede formation of aggregate by either E_3 or E_4 routes of aggregation. From the post-T_m data fit of Figure 5A, an activation energy of 28 kcal/mol was obtained. This activation energy was ascribed to a change in aggregation rate that depended upon unfolding. Although tempting to attribute this 28 kcal/mol activation energy to E_3 as described by the Lepock model, we have found that the theory contained in our model presents a more complex picture of the transition states post-unfolding. As temperature exceeds the T_m, k_4 becomes dominant, overtaking k_3 even though the activation energy barrier is greater than E_3. It is important to realize that the U state is sufficiently populated to supply both D_1^* and D_2^* at or above the T_m (up to 70 °C). The reaction pathway driven by k_3 and k_4 is no longer rate-limited by k_1. Hence the rate k_3 becomes less prominent, while k_4 becomes the rate-determining factor post-T_m as described in Figure 6 even though its activation energy is greater than the same for k_3. The result leads to a reasonable fit of the data as depicted in Figure 5B.

The results of the calculated C_P and the measured C_P for different scanning speeds are shown in Figure 3. It can be seen that there is good agreement between eq 31 and the experimental data. The kinetic rate constants span a range of more than 10 orders of magnitude (Figure 6). For that reason, we have a system of stiff differential equations to solve (Matlab ODE solver *ode*15*s* was used). The temperature where k_1 and k_2 cross corresponds to the T_m (~53.5 °C) for a fully reversible unfolding system that involves only the native and unfolded states.

Table 2. Comparison of Initial Rate Predicted at 34 °C for the 2 mg/mL Solution by Different Methods[a]

	expt	Sánchez-Ruiz	pre-T_m fit	eq 21
rate (M/s)	8.5×10^{-13}	3.8×10^{-12}	6.3×10^{-13}	6.2×10^{-13}

[a] For the pre-T_m fit, see Figure 5A. The rate for the model is calculated by converting equation 21 to the correct units.

Table 3. Comparison of Total Enthalpy Measured (Top Row), Approximation from eq 37 (Middle Row), and the Simulated Values from eq 31 (Bottom Row)

v (deg/min)	0.25	0.5	1.0	1.5	
eq 36	128	129	138	130	kcal/mol
eq 37	123	131	141	147	kcal/mol
eq 31	125	131	138	140	kcal/mol

The comparison of calculated aggregation based on the model and the experimentally obtained SEC data is shown in Figures 4 and 5B. Note that the temperature associated with each data point has a variability of ±1 °C as shown in the plot. Regarding the calculated results shown in Figure 4, the curves above T_m are calculated from an initial condition $N(t = 0) = 1$, $U(t = 0) = D_1(t = 0) = D_2(t = 0) = 0$ assuming a linear heating time of 60 s from $T_0 = 25$ °C, while the curves below T_m were calculated with an equilibrium between N and U at $t = 0$, i.e., $N(t = 0)/U(t = 0) = k_2/k_1$.

A comparison of the initial rate obtained from the time−temperature experiment at 34 °C to the rates obtained by three different methods is listed in Table 2. The aggregation rate predicted by the model (eq 21) and the pre-T_m fit best represents the experimentally determined aggregation rate in comparison to the Sánchez-Ruiz model.

There is another check for the consistency of all our parameters: the total heat (enthalpy) of the reaction. The experimental measurement can be directly calculated by:

$$\Delta H = \int_{T_F}^{T_0} C_p \, dT \tag{36}$$

where T_0 and T_F are the beginning and final temperatures of the transition envelope. From eq 31, we can obtain an approximate expression for this quantity:

$$\Delta H \approx (E_1 - E_2) + E_3 \cdot D_1 + 2E_4 \cdot D_2 \tag{37}$$

where $E_1 - E_2 = \Delta H_m$, the unfolding reaction enthalpy. D_1 and D_2 are obtained at the end of our numerical integration of eqs 6−8. The comparison is shown in Table 3. It is noted that

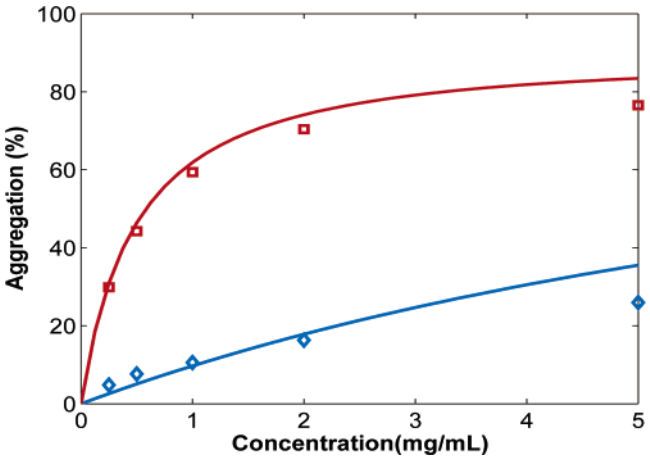

Figure 7. Comparison of the concentration dependence of rhuIL-1R(II) aggregation predicted by the model using the parameters extracted. The curves depict the behavior predicted by the model, and the data points represent measured aggregation by SEC. The upper curve and points correspond to data at 67.5 °C for a duration of 2 min. The lower ones correspond to data at 42.5 °C for 48 h.

there is good agreement in ΔH between the experimental and calculated results.

All the experimental data discussed thus far were obtained with a fixed concentration of 2 mg/mL. Interestingly, the model can be applied to describe the concentration dependence of the aggregation rate (eqs 12 and 13). Figure 7 shows the predicted and the experimentally determined concentration response at two different temperatures corresponding to different time durations. It shows the simple assumption that k_3 depends linearly on the concentration works fairly well at the lower concentration range but tends to overestimate aggregation rates at higher concentrations. Why it deviates from the experimental results more significantly at the highest concentrations tested is unclear. A possible explanation may be that at higher concentrations there is a greater tendency for the protein to self-associate in the solution phase. Such molecular crowding as the protein concentration is increased can lead to an augmentation of aggregation.[34,35] However, a portion of noncovalent self-associated aggregates can be reversible entities in solution that are not picked up by the SEC method and therefore may be observed lower than what actually exists in solution. This could occur as a result of dilution or during passage through the size exclusion column.[34] The disparity between aggregation in solution and that determined by SEC would then be expected to increase with concentration where the theoretical prediction exceeds SEC aggregation results.

4.3 Discussion. A major hurdle to overcome is the lack of ability to make reasonable estimates of aggregation half-life at conditions of low temperature storage. Storage conditions of marketed liquid biopharmaceuticals normally require refrigerated temperatures. Most of the approaches used in this context have relied upon empirical modeling methods.[29] Although these methods have applied Arrhenius models to make predictions about shelf life, they have ignored the thermodynamic properties of reactions that can often result in non-Arrhenius behavior. In the study presented, a mechanistic model has been proposed to predict properties of shelf life as it pertains to aggregation. This model has been applied to better evaluate non-Arrhenius reaction rates of rhuIL-1R(II) aggregation mediated by unfolding. In this first step taken, the validity of the simulation in regard to appropriately predicting the influence of concentration factors, deriving respectable thermodynamic parameters from a partially irreversible process, and emphasizing protein unfolding as a prerequisite to aggregation has successfully explained the aggregation kinetics of the system.

The thermal unfolding enthalpy in the absence of urea exhibited more heat (~48 kcal/mol) than could be accounted for in the reversible case (with urea). We have considered other alternative modeling schemes to explain these results such as different unfolded or U states where the enthalpy with urea was lower than the enthalpy in its absence (as dictated by the experimental results). Although one could still obtain a fit, it was not as good as the proposed model and there were other issues. For example, in the case of altered unfolded states, $\Delta H_m \neq E_1 - E_2$, and the expectation that it should be a valid equality has been suggested by Lepock and co-workers.[16] Additionally, when k_3 and k_4 were made equal to zero (as in the fully reversible case), the theoretical T_m was ~65 °C (above the highest scan T_m), a condition that does not satisfy and is far removed from the fully reversible case in urea (~52.6 °C). Furthermore, the heat gained does coincide with the population of states $\geq T_m$ where massive aggregation has been confirmed in both the "time−temperature" SEC studies as well as those studies conducted in the calorimeter (in addition to the presence of a deconvoluted peak at ~60 °C under the unfolding transition on the high-temperature side that is close to the 48 kcal/mol enthalpy increase). In contrast, by adopting the theory as presented here in this article, greater harmony was found among the experimental observations (i.e., better fit of the data), where the 48 kcal/mol increase in enthalpy could be assigned to a deconvoluted peak on the high-temperature side representing contributions from the D states (D_1 and D_2). Moreover, ΔH_m more appropriately agreed with the $E_1 - E_2$ equality (~74.3 kcal/mol instead of ~54 kcal/mol; closer to the 82 kcal/mol in the urea case). When k_3 and k_4 were set to zero, the T_m was approximately ~53.5 °C, much closer to the value in urea but slightly higher as would be anticipated when chemical denaturant is absent. We examined the case where only a second-order aggregation process was simulated and found an unfavorable ΔH_m of ~52 kcal/mol and a predicted T_m of 51 °C. These values are not valid since they were not consistent with the measured enthalpy and T_m values in the DSC experiment using urea.

The corresponding transition states (D_1^* and D_2^*) of the D state are inferred from the observation of a noticeable change in kinetics above the T_m. This temperature zone coincides with more rapid aggregation kinetics (massive) than what was observed at temperatures below the T_m. It testifies to the validity of a constant supply of unfolded protein that can rapidly interact by either a first- or second-order mechanism. Furthermore, justification for E_4 is found by the quality of fit on the high-temperature side of the DSC endotherm.

The relationship between activation energy and total enthalpy of the unfolding transition described by Sánchez-Ruiz et al.[11] and Lepock et al.[16] was found inadequate as an appropriate description of the DSC behavior of rhuIL-1R (II). Moreover, they did not include influences of the ΔC_P that contribute to

(33) Sturtevant, J. M. *Proc. Natl. Acad. Sci. U.S.A.* **1977**, *74*, 2236−2240.
(34) Shire, S. J.; Shahrokh, Z.; Liu, J. *J. Pharm. Sci.* **2004**, *93*, 1390−1399.
(35) Zimmerman, S. B.; Minton, A. P. *Annu. Rev. Biophys. Biomol. Struct.* **1993**, *22*, 27−65.

non-Arrhenius aggregation responses. Although the ΔC_P does not contribute significantly within the temperature regime in the vicinity of the T_m, it can pose more influence at lower temperature. In contrast to these approaches, the present work has derived a theoretical treatment that can be applied to DSC data to extract thermodynamically meaningful parameters from a partially reversible system. Unlike the work of Sánchez-Ruiz et al. and Lepock et al., this work describes the system in terms of both first- and second-order reaction properties that depend on the thermodynamics of unfolding. It takes into account the influences of the denaturational heat capacity in describing the non-Arrhenius kinetics of aggregation that can occur at low as well as high temperatures. Finally, it satisfactorily describes the enthalpy and activation energies along the aggregation reaction pathway and lays the groundwork for predicting shelf life of complex protein aggregation systems.

5. Conclusions

The validity of the model in extracting meaningful thermodynamic parameters in a partially reversible system is determined by the capability of the model to determine these parameters uniquely. The level of sophistication in the model imposes limitations on the results. For example, if the model has too few parameters, one may either get a poor fit or forego certain detailed description of the system. On the other hand, if there are too many parameters, a good fit may not ensure a unique set of parameters and therefore render them meaningless. Although global identifiability is difficult to achieve, we checked the local identifiability of our model by the rigorous calculation described in Section 3.3 and showed that our calculated parameters were uniquely determined. From the results, we were able to extract meaningfully relevant thermodynamic (e.g., ΔC_P, ΔH_m, and T_m) and kinetic parameters (e.g., A_1, E_1, A_2, E_2, A_3, E_3, A_4, and E_4) with varying levels of certainty. Two factors contribute to the uncertainty of the parameters we obtained. The first is the uncertainty in measurements. The second is the intrinsic sensitivity of the observables to each parameter under the conditions of the experiment. To estimate the uncertainties of the parameters in the model, we considered a 10% error in protein concentration. Correspondingly, the uncertainties induced by this error in the parameter estimations can be determined by projecting the error on the expectation space of theoretical observables. As a result, the quantity with the largest uncertainty is E_2, as shown in Table 1. This is expected since k_2 is the least dependent on temperature among all the kinetic coefficients. Therefore, in the limited temperature range of the experiment, we could not determine the value of E_2 and A_2 very well. However, despite this difficulty, we could still determine ΔH_m and T_m relatively well. As suggested by this study, we expect improvement could be achieved if we expanded the study to include slower and faster DSC scan rates than those examined in the study. A more definitive improvement can be achieved if E_2 could be measured directly in a separate experiment.

We believe that the model presented, though not perfect, captures the main physical processes underlying the experimental conditions tested. Several points can now be made concerning the approximations and assumptions used as they pertain to real molecular properties. The model as presented tends to support the $\Delta H_m = E_1 - E_2$ expectation.[16] It can account for the additional 48 kcal/mol in the total enthalpy of the partially reversible system by allowing for populated *D* states (of aggregation) on the high-temperature side of the unfolding envelope. This is supported by the massive aggregation observed at temperatures greater than or equal to the T_m. When k_3 and k_4 are set equal to zero to simulate the fully reversible case based on the theory, the T_m ($\sim$53.5 °C) is very near that observed experimentally for the reversible case in urea ($\sim$52.6 °C). The assumption that a combination of first- and second-order reaction rates are involved in the aggregation kinetics is supported by the experimental findings that the reaction order is $\sim 1.70 \pm 0.04$. Finally, a reasonable prediction of aggregation rates at low temperatures (below the unfolding transition) was achieved taking into account curvature imposed by the ΔC_P term used in the theoretical treatment. There is no question that further refinements based on more experimental evidence will help determine the mechanism and parameters more accurately so that extrapolation to other temperatures (above and below the T_m) result in meaningful predictions. The experimental findings suggest that stability of rhuIL-1R (II) is afforded through the thermodynamic stabilization of the native state as suggested below the T_m, or by stabilizing the unfolded state where progress to the irreversibly denatured aggregate is effectively blocked as in the case of the urea experiment. Furthermore, unfolded or conformationally altered protein propagate the aggregation reaction for this system.

It is anticipated that this model could be applied to better predict levels of aggregation at low temperatures. This aspect has significant implications with regard to fulfilling a need regarding better estimations of shelf life for biopharmaceuticals. Furthermore, the model appropriately describes aggregation conditions associated with varying concentration factors. Hence, it is possible to run scan-rate-dependent experiments at a single concentration in the calorimeter and translate the results into meaningful estimates that predict aggregation kinetics at other concentrations.

Acknowledgment. We are grateful for the helpful assistance of Mary Wallace, who generated the DSC and SEC data used in this work. Additionally, it is of special significance to thank Duke Phan for his discovery of the conditions whereby rhuIL-1R was found to be reversible in urea.

JA043466G